# Volume-grating Stokesmeter based on photonic bandgap structures

Jong-Kwon Lee, Xue Liu, and M. S. Shahriar

Center for Photonic Communications and Computing, Department of Electrical Engineering and Computer Science, Northwestern University, 2145 North Sheridan Road, Evanston, Illinois 60208, USA

*Corresponding author: jklee7@msn.com

Received 28 October 2008; accepted 15 April 2009;
posted 23 April 2009 (Doc. ID 103292); published 5 June 2009

An inherent polarization sensitivity of a volume grating, in general, can be used to determine all the Stokes parameters of input beams. We demonstrate the polarization-dependent bandgap in a photonic crystal in principle at any wavelength using the finite-difference time-domain method. We show how this bandgap can be used to realize a volume-grating Stokesmeter. We also present an explicit design for a high-speed version of such a Stokesmeter and identify design constraints that arise in this context. Finally, we describe a spectrally resolved volume-grating Stokesmeter based on the tunability of a photonic bandgap material. © 2009 Optical Society of America

*OCIS codes:* 050.7330, 110.5405, 230.0230.

## 1. Introduction

Polarization imaging [1–3] can discriminate an object from its background in situations where conventional imaging methods fail. Identifying the Stokes vector components of the polarization of light reflected from an object allows one to construct an image that corresponds to the target's unique polarimetric signature [4]. This is useful in applications ranging from target recognition to vegetation mapping [5–7]. Current polarization imaging systems, including mechanical quarter-wave plate/linear polarizer combinations, photodetectors with polarization filtering gratings etched onto the pixels, and liquid crystal variable retarders [8–10], can be limited in speed or by the lack of an ability to determine the complete Stokes vector. A holographic Stokesmeter (HSM) [11] uses the polarization dependence of volume-grating diffraction efficiencies to determine all four Stokes parameters in parallel and at a high speed. However, the current HSM cannot be used for a wide frequency range due to the limitations of thick holographic materials.

0003-6935/09/173212-04$15.00/0


The polarization-dependent bandgap characteristics have been experimentally observed for propagation in the plane of periodicity in both slab and bulk two-dimensional (2D) photonic crystals (PCs) [12,13], and has been used to create novel wave plates and polarization beam splitters [14]. The polarization-dependent properties of PCs can be tailored by adjusting the lattice geometry, size, and dimensionality, as well as the refractive indices of the constituent materials. Thus, PCs are more versatile than conventional devices in controlling polarization. In addition, since Maxwell's equations are scale invariant, results obtained at one portion of the electromagnetic spectrum apply equally well across the entire spectrum with appropriate scaling of the structure. Therefore, if we can implement a volume-grating polarimeter using these properties of a PC, such devices can be operated over a wide range of frequencies.

In this paper, we investigate the inherent polarization sensitivity of a volume grating in the form of a PC at any wavelength using the finite-difference time-domain (FDTD) method. We then present an explicit design to realize a high-speed version of a volume-grating Stokesmeter using this polarization-dependent photonic bandgap (PBG) structure. Finally, we describe a spectrally resolved

volume-grating Stokesmeter based on the tunability of a PBG system.

### 2. Polarization-Dependent Photonic Bandgap

The 2D PBG structure we simulate for the Stokesmeter consists of six rows of 4 mm diameter Pyrex rods ($\varepsilon_r = 4.2$) on a 9 mm square lattice, as illustrated in Fig. 1(a). The structure is assumed to extend to infinity in the $y$ and $z$ directions with no charge. The incident wave, into the PBG structure along the $x$ axis, is assumed uniform in the $z$ direction, so that all partial derivatives of the fields with respect to $z$ equal to zero. We simulate a light wave function normally incident (i.e., no $E_x$ or $H_x$ component) upon a slab with infinite extent in the $y$ and $z$ directions by placing one unit slab of the PC in the computational cell, as shown in Fig. 1(b). The FDTD simulation is performed for both $z$-polarized (i.e., $E_y = 0$) and $y$-polarized (i.e., $E_z = 0$) light by sending a single pulse of light with a wide frequency profile multiplied by a sinusoidal wave through the PC. The output amplitudes are calibrated at a record point after the PC with and without the PC. By performing a discrete Fourier transform for both transmitted and incident amplitudes, we get the transmission spectrum, as shown in Fig. 2. Deep absorptions in the frequency ranges of 12 to 15 and 23 to 26 GHz are observed for the $z$-polarized case. For the $y$-polarized case, a shallow absorption around 17 GHz and a deep absorption around 27 GHz are produced.

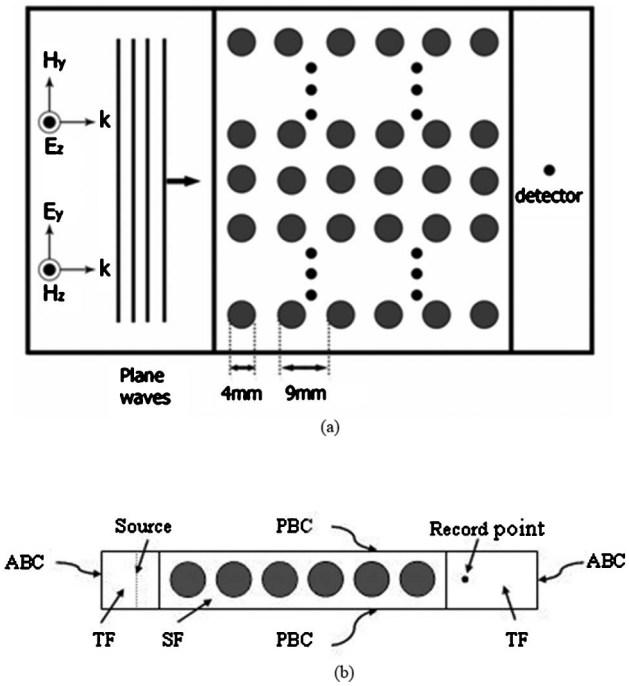


Fig. 1. (a) Two-dimensional photonic crystals that consist of six rows of 4 mm diameter Pyrex rods ($\varepsilon_r = 4.2$) on a 9 mm square lattice. The $z$-polarized and the $y$-polarized light is incident on the PBG structure along the $x$ axis. (b) Schematic diagram for PBG calculation (TF, total field; SF, scattered field; PBC, periodic boundary condition; ABC, absorbing boundary condition; Source, Gaussian pulse × sinusoidal function)

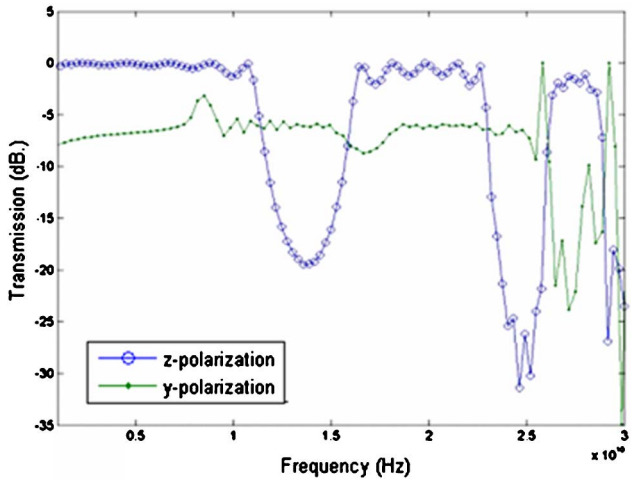


Fig. 2. Photonic bandgaps for $z$-polarized and $y$-polarized input beams for an array of 4 mm diameter Pyrex rods ($\varepsilon_r = 4.2$) on a 9 mm square lattice.

An arbitrary linear-polarization state of the input beam is easily produced by rotating the direction of the electric field in the $yz$ plane. By performing a FDTD simulation for such a beam, we find the transmission spectrum of this PBG structure has a significant dependence on the polarization state of the input beam, as illustrated in Fig. 3. As the angle of polarization of the incident wave in the $yz$ plane increases from 0° to90° (i.e., from $z$ polarization to $y$ polarization), the absorption dip becomes shallower. The transmission with respect to the linear-polarization states are plotted for two sample frequencies inside the bandgap (14 and 15 GHz), as shown in Fig. 4, which are qualitatively similar to the polarization-dependent diffraction efficiency from a volume holographic grating [15].

We define the contrast ratio (CR) as

$$\mathrm{CR} = \frac{T_{\max} - T_{\min}}{T_{\min}},$$

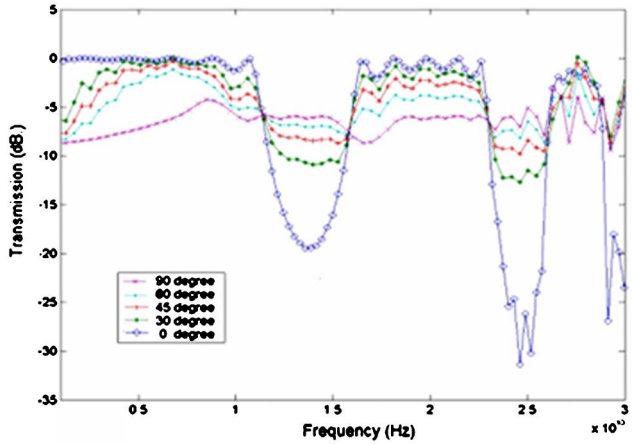


Fig. 3. Photonic bandgaps for different linear-polarization states with respect to the $z$-axis for an array of 4 mm diameter Pyrex rods ($\varepsilon_r = 4.2$) on a 9 mm square lattice.

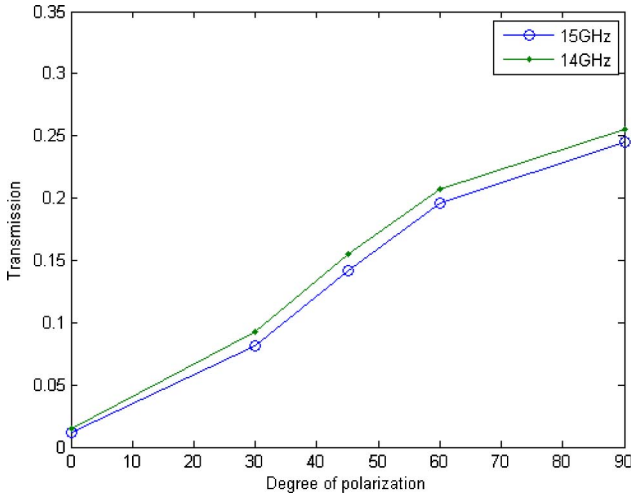


Fig. 4. (Color online) The transmission of different linear-polarization states for two different frequencies (e.g., 14 and 15 GHz) in the bandgaps.

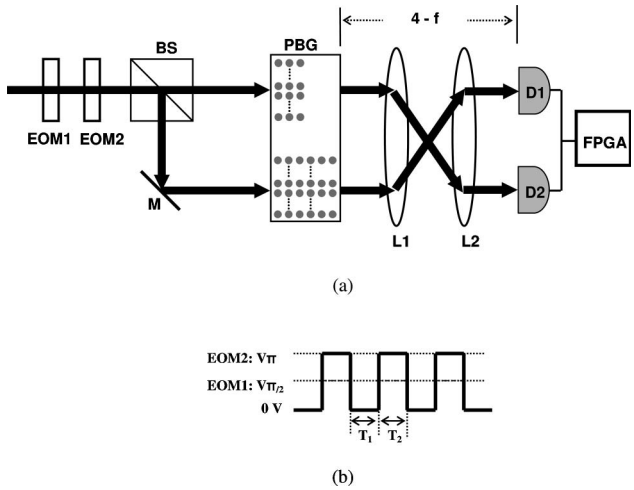


Fig. 5. (a) Proposed architecture for a PC-based volume-grating Stokesmeter. (b) Input voltage signal scheme of two EOMs (EOM, electro-optic modulator; PBS, polarization beam splitter; PBG, photonic bandgap material; M, mirror; L, lens; D, detector; FPGA, field programmable gate array).

where $T_{\max}$ and $T_{\min}$ denote the maximum and minimum transmission, respectively. As seen in Fig. 4, for a frequency component at 14 GHz (15 GHz), the transmission varies from 0.012 (0.014) at 0° to 0.245 (0.256) at 90°, resulting in a CR of 95.2% (94.1%). Note that the simulated PC model consists of only six rows of aluminum rods. In reality, more rows of rods can be implemented to assure an almost 100% absorption at this frequency, meaning that this PBG structure may be used as a polarimeter with a nearly perfect contrast ratio.

### 3. Volume-Grating Stokesmeter

Based on the polarization sensitivity of the PBG structure, we propose a volume-grating Stokesmeter, as shown in Fig. 5(a), that consists of a pair of spatially separated volume gratings in a PC, two electro-optic modulators (EOMs), and an imaging system.

The basic structure of this device is almost the same as the compact version of a holographic Stokesmeter [16], except that the volume gratings in a holographic material are replaced with the ones in a PC. The first and second EOMs play the role of a quarter-wave plate and a half-wave plate, respectively. The fast axis of the second EOM is rotated 45° with respect to that of the first EOM. In order to determine the Stokes vector of the input beam, the transmitted beam is measured twice separately at two time periods ($T_1$ and $T_2$), as shown at the bottom of Fig. 5(b). During the interval $T_1$ ($T_2$), the EOMs are turned off (on). $I_{t1}$ ($I_{t2}$) indicate the intensity transmitted through the top (bottom) volume grating during the interval $T_1$. Similarly, $I_{t3}$ ($I_{t4}$) indicates the intensity transmitted through the top (bottom) volume grating during the interval $T_2$. $A_i$ ($B_i$) characterizes the diffraction efficiency of the $i$th (1, top; 2, bottom) grating for the $z$-polarized ($y$-polarized) input light. The angle $\gamma_1/\gamma_2$ denotes the rotation of the substrate containing the first/second grating around the $x$ axis in the clockwise direction when looking in the $+x$ direction. By measuring all four transmitted beam intensities for a specific frequency in a PBG during intervals $T_1$ and $T_2$, we can find the input Stokes parameters, as we did for the HSM [16], through the following measurement matrix:

$$\begin{bmatrix} I_{t1} \\ I_{t2} \\ I_{t3} \\ I_{t4} \end{bmatrix} = \begin{bmatrix} A_1 + B_1 & (A_1 - B_1)\cos(2\gamma_1) & (A_1 - B_1)\sin(2\gamma_1) & 0 \\ A_2 + B_2 & (A_2 - B_2)\cos(2\gamma_2) & (A_2 - B_2)\sin(2\gamma_2) & 0 \\ A_1 + B_1 & -(A_1 - B_1)\cos(2\gamma_1) & 0 & (A_1 - B_1)\sin(2\gamma_1) \\ A_2 + B_2 & -(A_2 - B_2)\cos(2\gamma_2) & 0 & (A_2 - B_2)\sin(2\gamma_2) \end{bmatrix} \begin{bmatrix} I \\ Q \\ U \\ V \end{bmatrix}. \quad (1)$$

Here, ($I$, $Q$, $U$, $V$) represents the input Stokes parameters.

We point out that, if $\gamma_1 = \gamma_2$, different contrast ratios between the $z$- and $y$-polarized light are required for the gratings in Figs. 5(a) and 5(b). This can be seen mathematically from Eq. (1): the determinant of the measurement matrix vanishes if $A_1 = A_2$, $B_1 = B_2$, and $\gamma_1 = \gamma_2$. The volume-grating elements

in this system can be a pair of spatially separated PBGs with two different numbers of rows of rods. Alternatively, these elements can be constructed with a pair of spatially separated PBG structures, where the diameters of the rods are different, but the distances between the rods are the same. Either way, we can create the polarization-dependent transmission spectrum for a specific frequency with two different contrast ratios of the transmitted beam intensities for $y$ and $z$ polarizations. Another alternative is to use different values of $\gamma_1 = \gamma_2$.

It is also possible to implement a spectrally resolved volume-grating Stokesmeter [17] based on such PBG structures. Researchers have recently developed many structures activated by several external parameters, including electric field, magnetic field, and strain, to implement tunable band stops in PBGs [18–20]. The tunability of bandgaps is usually achieved by controlling the electric permittivity or the magnetic permeability of the constituent materials since the bandgap positions are governed by the average refractive index of the composite. Thus, by using one of these methods to realize a tunable PBG structure in our architecture, it should be possible to implement a PBG-based spectrally resolved polarimeter. Compared to the classic polarization imaging systems, in which the mechanical rotations between the wave plate and the polarizer are needed for determining each Stokes parameter, the new imaging system works at a much faster speed.

## 4. Conclusion

We have demonstrated a polarization-dependent photonic bandgap in a 2D PC structure at any wavelength using the FDTD. We have then proposed a volume-grating Stokesmeter based on the polarization sensitivity of a pair of spatially separated PBG structures and have discussed the basic principle of this device. This PBG-based Stokesmeter can be operated in a wide frequency range with appropriate scaling of the PBG structures and can be used to realize a polarimeter with a nearly perfect contrast ratio. Moreover, we can implement a spectrally resolved volume-grating Stokesmeter using the tunability of PBG structures.

## References


1. J. L. Pezzaniti and R. A. Chipman, "Mueller matrix imaging polarimetry," Opt. Eng. **34**, 1558–1568 (1995).
2. K. P. Bishop, H. D. McIntire, M. P. Fetrow, and L. McMackin, "Multispectral polarimeter imaging in the visible to near IR," Proc. SPIE **3699**, 49–57 (1999).
3. G. P. Nordin, J. T. Meier, P. C. Deguzman, and M. W. Jones, "Micropolarizer array for infrared imaging polarimetry," J. Opt. Soc. Am. A **16**, 1168–1174 (1999).
4. L. J. Denes, M. Gottlieb, B. Kaminsky, and D. Huber, "Spectropolarimetric imaging for object recognition," Proc. SPIE **3240**, 8–18 (1998).
5. A. Gerrard and J. M. Burch *Introduction to Matrix Methods in Optics* (Dover, 1974).
6. L. D. Travis, "Remote sensing of aerosol with earth-observing scanning polarimeter," Proc. SPIE **1747**, 154–164 (1992).
7. G. L Brun, B. L. Jeune, J. Cariou, and J. Lotrian, "Analysis of polarization signature of immersed target," Proc. SPIE **1747**, 128–139 (1992).
8. T. Nee and S. F. Nee, "Infrared polarization signature for targets," Proc. SPIE **2469**, 231–241 (1995).
9. P. J. Curran, "Polarized visible light as an aid to vegetation classification," Remote Sens. Environ. **12**, 491–499 (1982).
10. J. Chen, T. N. Pappas, A. Mojsilovic, and B. E. Rogowitz, "Adaptive perceptual colo-texture image segmentation," IEEE Trans. Image Process. **14**, 1524–1536 (2005).
11. M. S. Shahriar, J. T. Shen, R. Tripathi, M. Kleinschmitt, T. Nee, and S. F. Nee, "Ultrafast holographic Stokesmeter for polarization imaging in real time," Opt. Lett. **29**, 298–300 (2004).
12. E. Chow, S. Y. Lin, S. G. Johnson, P. R. Villeneuve, J. D. Joannopoulos, J. R. Wendt, G. A. Vawter, W. Zubrzycki, H. Hou, and A. Alleman, "Three dimensional control of light in two dimensional photonic crystalslab," Nature **407**, 983–986 (2000).
13. J. M. Hickmann, D. Solli, C. F. McCormick, R. Plambeck, and R. Y. Chiao, "Microwave measurement of the photonic band gap in a two dimensional photonic crystal slab," J. Appl. Phys. **92**, 6918–6920 (2002).
14. D. R. Solli, C. F. McCormick, R. Y. Chiao, and J. M. Hickmann, "Polarization control using photonic crystals," Opt. Photon. News **14**(12), 35 (2003).
15. M. S. Shahriar, J. T. Shen, M. A. Hall, R. Tripathi, J-.K. Lee, and A. Heifetz, "Highly polarization-sensitive thick gratings for a holographic Stokesmeter," Opt. Commun. **245**, 67–73 (2005).
16. J.-K. Lee, J. T. Shen, A. Heifetz, R. Tripathi, and M. S. Shahriar, "Demonstration of a thick holographic Stokesmeter," Opt. Commun. **259**, 484–487 (2006).
17. J.-K. Lee, J. T. Shen, A. Heifetz, and M. S. Shahriar, "Demonstration of a spectrally scanned holographic Stokesmeter," Opt. Commun. **277**, 63–66 (2007).
18. B. Li, J. Zhou, L. Li, X. J. Wang, X. H. Liu, and J. Zi, "Ferroelectric inverse opal with electrically tunable photonic band gap," Appl. Phys. Lett. **83**, 4704–4706 (2003).
19. M. Golosovsky, Y. Saado, and D. Davidov, "Self-assembly of floating magnetic particles into ordered structures," Appl. Phys. Lett. **75**, 4168–4170 (1999).
20. S. Kim and V. Gopalan, "Strain-tunable photonic band gap crystals," Appl. Phys. Lett. **78**, 3015–3017 (2001).